Journal of Engineering Science and Technology
Vol. 12, No. 12 (2017) 3173 - 3187

FABRICATION AND UTILIZATION OF ZINC OXIDE NANOFIBRES FOR SEMICONDUCTORS OF PHOTOVOLTAIC- AND PIEZOELECTRIC-BASED HYBRID GENERATORS

SUYITNO[1,*], ATMANTO HERU WIBOWO[2], MIRZA YUSUF[3], DIDIN MUJAHIDIN[4], DOMINICUS DANARDONO[1]

[1]Department of Mechanical Engineering, Universitas Sebelas Maret, Jl. Sutami 36A Surakarta, Indonesia
[2]Department of Chemistry, Universitas Sebelas Maret, Jl. Sutami 36A Surakarta, Indonesia
[3]Department of Mechanical Engineering, Vocational Program, Universitas uhammadiyah Yogyakarta, Jl. Ring Road Barat, Tamantirto, Kasihan, Bantul, Yogyakarta
[4]Department of Chemistry, Institut Teknologi Bandung, Jl. Ganesha 10, Bandung, Indonesia
*Corresponding Author: suyitno@uns.ac.id

Abstract

The objective of this study is to develop and test hybrid generators harvesting both solar and mechanical energy. The hybrid generators work using photovoltaic- and piezoelectric-principles, where the active semiconductors were ZnO nanofibres synthesized by electrospinning at various feed rates of precursor. The results show that the crystallinity, crystalline size, fibre size, and fibre uniformity examined by X-ray diffraction and scanning electron microscopy were strongly affected by changing the solution flow rate among 2, 4, 6, and 8 μL/min. Meanwhile, the voltage and power generated from the hybrid generators were influenced by the crystalline quality and morphology of the ZnO fibres. The highest voltages of photovoltaic- and piezoelectric-based hybrid generators were 507 and 36.3 mV, respectively. In addition, the maximum power values of photovoltaic- and piezoelectric-based generators were 706.72 μW/cm² and 49.6 nW/cm², respectively. Therefore, hybrid generators are of interest for fabrication into self-power devices.

Keywords: Nanofibre, Semiconductors, Piezoelectric, Photovoltaic, Hybrid nanogenerator.

1. Introduction

Small devices for harvesting renewable energy are of much interest for personal electronics, personal computers, and sensors. Currently, such devices are driven by batteries or capacitors requiring periodic charging from external energy. Self-

Nomenclatures

A	Active area, m²
D	Size of the crystal
G	Irradiance intensity, W/m²
h	Planck's constant, $6.626 \cdot 10^{-34}$ Js
I_{mpp}	Current at the maximum power point, A
k	A constant, 0.9
P_L	Output power, Watt
P_{max}	Maximum output power, Watt
R_L	Electric load, Ω
T	Period, s
V_{mpp}	Voltage at maximum power point, Volt
V_o	Output voltage, Volt
v	Frequency

Greek Symbols

α	Absorbance
β	Full width at half maximum intensity
η	Efficiency of the solar cell
θ	Diffraction angle
λ	Wavelength

Abbreviations

CoAc	Cobalt Acetate
DSSC	Dye-Sensitized Solar Cell
FTO	Fluorine-doped Tin Oxide
FWHM	Full Width at Half-Maximum
NG	Nanogenerator
PVA	Polyvinyl Alcohol
PVDF	Polyvinylidene Fluoride
PVP	Polyvinyl Pyrrolidone
PZT	Lead Zirconate Titanate
SEM	Scanning Electron Microscopy
TiO_2	Titanium Dioxide
XRD	X-Ray Diffraction
ZnAc	Zinc Acetate
ZnO	Zinc Oxide

powered nanogenerators (NGs) have been developed not only using a single energy source [1-10] but also using various energy sources [11-13]. Therefore, one of the key issues is how to harvest electricity from multiple renewable energy sources in a single and compact nanogenerator device.

NGs are mainly fabricated from semiconductors. TiO_2 has been intensively studied for dye-sensitized solar cells (DSSCs) because it produces superior performance compared to that produced by ZnO-based DSSCs. In contrast, the uniqueness of non-centrosymmetric ZnO crystals may produce a piezoelectric effect. To date, lead-free materials such as ZnO [14], $0.755(Bi_{0.5}Na_{0.5})TiO_3$-$0.065BaTiO_3$-$0.18SrTiO_3$ (BNT-BT-ST) [15], polyvinylidene fluoride (PVDF) [16],

and $(K_{0.5}Na_{0.5})NbO_3$ [17] have been intensively developed for piezoelectric materials. In addition, ZnO, with some other unique properties including a wide energy band gap of 3.61 eV [18], intrinsic n-type semiconductivity, and resistance to high temperatures, has been used for the construction of various equipment, e.g., solar cells [19-21], gas sensors [22, 23], and piezoelectric-based devices [24-28]. Unfortunately, the ability of ZnO to act as a semiconductor in energy conversion devices is still limited to a single source. Thus, the study of ZnO in hybrid devices proves to be an interesting topic.

ZnO-based NGs have been studied using nanowires [8], nanorods [14], and nanotubes [9] as a single energy source. Moreover, hybrid NGs have also been developed using CdSe combining piezoelectric and photoelectric concepts [12], using nanopillars for solar cells and PVDF for the piezoelectric effect [29], using piezoelectric and triboelectric effects [30], and using ZnO nanosheets for organic photovoltaic and piezoelectric NGs [31]. To the best of our knowledge, although different types of hybrid devices have been developed, hybrid NGs for harvesting solar energy using the concept of dye-sensitized solar cells (DSSCs) and mechanical energy using the piezoelectric effect have not been reported, except from Kim et al. [32]. The hybrid NGs used flexible DSSCs, whereas the semiconductors used were ZnO nanorods. Meanwhile, the piezoelectric effect was accomplished by bending loads. An efficiency of 0.69% with J_{sc} (3.95 mA/cm²) and V_{oc} (0.65 V) were produced when hybrid NGs worked as DSSCs [32]. In addition, an output voltage of approximately 1.5 V with an output current density approaching 80 nA/cm² was generated when hybrid NGs worked using the piezoelectric effect [32]. Unfortunately, the main type of mechanical load on the keyboards is a compressive load instead of a bending load.

Therefore, the objective of the study is to demonstrate and investigate the hybrid NGs for harvesting solar energy using the concept of DSSCs and mechanical energy using the piezoelectric effect, where the semiconductors used were ZnO nanofibres and the mechanical load used was a cyclic compressive load. For better understanding, the effects of the precursor feed rate in the electrospinning on the morphology, crystallite properties, and performance of hybrid NGs were also studied. The hybrid NGs have advantages in their design because they have just one active area and are therefore simple to manufacture. The fibres of ZnO fabricated by an electrospinning machine [33, 34] were attached onto conductive transparent glass by a screen-printing method.

2. Experimental Procedures

2.1. Materials

For synthesizing the fibres of ZnO, we used purified water, polyvinyl alcohol ($[-CH_2CHOH-]_n$, PVA 72000, Merck), zinc acetate dihydrate ($Zn(C_2H_3O_2)_2{\cdot}2H_2O$, ZnAc, Merck), and cobalt(II) acetate tetrahydrate ($(CH_3COO)2Co{\cdot}4H_2O$, CoAc, Merck). The materials were used as received. The precursor solution in the electrospinning machine is PVA-based with a molecular weight of 72,000, and it has a good enough viscosity and conductivity to form a Taylor cone and create fibres by using an electrostatic field.

2.2. Fabricating and testing the hybrid NGs

The hybrid NGs were fabricated from FTO (fluorine-doped tin oxide) glass, ZnO fibres attached onto the FTO glass, N719 dye solution, electrolytes, counter electrode glass, and a rubber sheet. The hybrids NGs, as shown in Fig. 1, were assembled as DSSCs, where the counter electrode was attached onto the rubber sheet as a flexible mounting. The counter electrodes could freely move upward and downward when the FTO glass was subjected loads.

FTO (fluorine-doped tin oxide) glass was synthesized by a previously reported method [35]. Meanwhile, the counter electrodes were made with the base substrate using FTO, where platinum was sputtered and deposited onto FTO. Platinum was placed in the vacuum room with a base pressure of 9.5 x 10^{-5} Torr, while argon gas was maintained at 4 mTorr before entering the vacuum space. The applied potential and current were 404 volts and 125 mA, respectively. The substrate was rotated at a speed of 5 rpm to produce a uniform deposition. The sputtering process for producing the counter electrode was carried out for 20 minutes. In addition, the preparation of the electrolyte and N719 dyes followed previous procedures [36].

To fabricate the hybrid NGs, the FTO glass with ZnO fibres was dipped in the N719 dye solution for 24 hours. Next, the FTO and counter electrode glass were attached and given a spacer with a distance of approximately 35 μm. Electrolytes were incorporated into the gap between the two glasses and then sealing was performed. The counter electrode glass was attached on the pliable rubber so that the ZnO semiconductor could be activated by applying the mechanical load. The order of layers of the hybrid NGs is shown in Fig. 1.

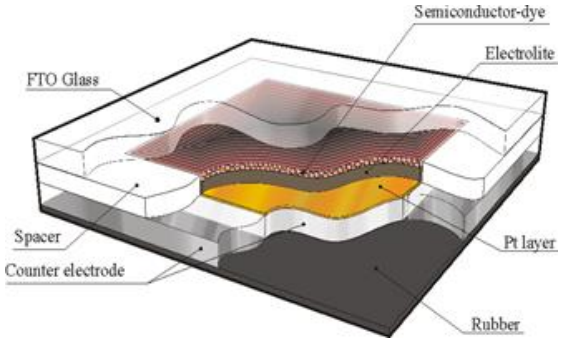

Fig. 1. Scheme of the hybrid NGs.

The ability of hybrid NGs to produce electrical energy by means of the piezoelectric effect was measured by an ADAM Advantech (series 4018) instrument, and the output voltage was read in real-time with the application of a compressive load at 0.5 kg. The load of 0.5 kg was applied to represent the condition of weak finger taps [37]. The power of piezoelectric-based NGs was then calculated using Formula 1 from the output voltage generated by providing the variation of the load resistance (Ω) [38].

$$P_L = \frac{1}{T}\int \frac{V_O(t)^2}{R_L}\, dt \quad (1)$$

The ability of hybrid NGs to produce electrical energy by means of the photovoltaic effect was measured by a solar simulator at an irradiance of 1000 W/m². The power of photovoltaic-based NGs was then calculated using Formula 2 from the point of maximum power (mpp, P_{max}). Meanwhile, Formula 3 calculated the efficiency of the hybrid NG based on the photovoltaic effect.

$$P_{max} = V_{mpp} I_{mpp} \tag{2}$$

$$\eta = \frac{P_{max}}{A \times G} \tag{3}$$

2.3. Synthesis and characterization of ZnO fibres

The ZnO fibres used for the photo anode in photovoltaic-based NGs as well as for the active layer in piezoelectric-based NGs were attached onto the FTO glass. The ZnO fibres were synthesized using electrospinning with a solution of zinc acetate (ZnAc) and poly vinyl alcohol (PVA). To synthesize the PVA solution, the PVA was dissolved in purified water at a mass ratio of 1:10. The PVA (2.0 g) and 20 mL of purified water were mixed and stirred until homogeneous at a temperature of 70°C for 4 hours, as mentioned previously [39]. The bubbles and foam were relieved for 24 hours at a temperature of 25°C.

To synthesize the solution of ZnAc, 2 g of ZnAc was mixed with 8 mL of purified water, stirred at a temperature of 70°C for 1 hour, and allowed to settle for 24 hours at a temperature of 25°C. The ZnAc/PVA solution was synthesized by mixing the ZnAc and PVA solutions at a weight ratio of 4:1. The last solution was mixed at a temperature of 70°C for 8 hours, followed by settling for 24 hours at a temperature of 25°C.

Moreover, 1.0 mL of ZnAc/PVA solution was put in the syringe pump, where the flow rates of the syringe pump in the horizontal electrospinning machine were 2, 4, 6, and 8 μL/min, respectively, and each solution was electrospun to produce the green ZnAc/PVA fibres. The collector of the electrospinning machine is FTO (fluorine-doped tin oxide) glass synthesized by a previously described method [35].

In addition, sintering of the green fibres was conducted at a temperature of 550°C for 2 hours to remove PVA because above 440°C, it was completely decomposed [40] and all that remained was the ZnO nanofibres. The morphology was characterized and crystallinity of the nanofibres was studied by scanning electron microscopy (SEM, FEI: Inspect-S50) and X-ray diffraction (XRD).

3. Results and Discussion

3.1. Morphology and crystallinity

Figure 2 shows SEM photographs of ZnO fibres synthesized by the electrospinning machine at various flow rates of precursor solution. It can be seen that the fibres are dense, long, absent of beads, rough, and have wires on their surface. Evidently, the long and dense fibres show that the ZnAc was well-dispersed in the PVA matrix and acted as nuclei in the conversion to ZnO crystals. The growth of ZnO crystals is localized, limited, and might coalescence within the PVA matrix [41]. Moreover, the formation of free beaded fibres means that the applied voltage and the precursor feed rate are sufficient to stretch the filaments from the needle tip to the FTO collector.

However, the produced fibres are different when compared with a previous study, where their fibres were grainy with the use of a precursor solution from ZnAc/PVP [33]. PVA is an atactic polymer [42], and therefore, it crystallises only to a very small extent because it lacks any regularity in the arrangement of substituents. Meanwhile, PVP contains almost equal proportions of isotactic and syndiotactic configurations [43]. In the syndiotactic configuration, the substituents have alternate positions along the chain. Meanwhile, in the isotactic configuration, all of the substituents are located on the same side of the macromolecular backbone. Due to their random nature, atactic PVA is usually amorphous. In contrast, isotactic and syndiotactic PVP are usually semi-crystalline. PVP is also a polymer possessing activity as a shape-control agent in the synthesis of nanocrystals [44, 45], promoting the growth of specific crystal faces while supressing the growth of others. In addition, the syndiotactic PVP also has a rapid rate of crystallization. Thus, the fibres synthesized by the electrospinning of ZnAc/PVP solution are grainy. Meanwhile, ZnO fibres synthesized using ZnAc/PVA precursors tend to be amorphous and covered by wires. This is also confirmed by the XRD spectra, in which high intensities occurred in the (101) and (100) crystal planes with moderate crystallinity.

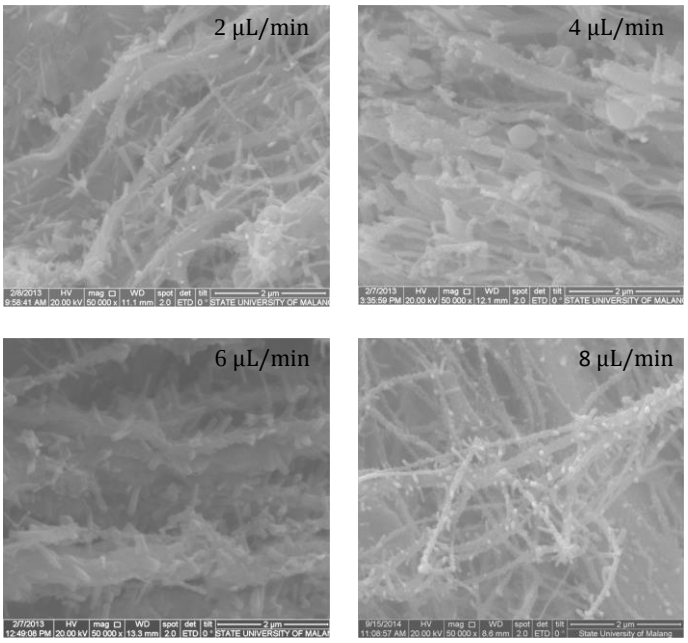

Fig. 2. SEM images of ZnO fibres at various flow rates of precursor solution into the electrospinning machine.

The diameter of the fibres is strongly affected by the precursor feed rate into the electrospinning machine [46]. Empirical observations indicate that the smallest diameters occur at the lowest flow rates, but the production rate and fibre size tend to vary with the solution concentration [47]. Increasing the precursor flow rate and decreasing the applied voltage tend to increase the fibre diameter and bead diameter [47] because the electric field cannot overcome the surface tension of precursors. By increasing the flow rate for the same electric field, the

average diameter of nanofibres increased due to the decrease of the charge in the unit volume of the precursor liquid [47, 48]. In addition, the diameter of ZnO fibres is also more homogeneous at a lower flow rate of precursor solution, as indicated by a smaller standard deviation and shown in Table 1. The smallest mean diameter of ZnO fibres is 142.7 nm, and it was obtained at a flow rate of 2 µL/min. It is important to note that the smallest flow rate is 2 µL/min because Taylor's cone and good fibres were very difficult to synthesize with the electrospinning machine with a needle diameter of 0.8 mm, applied voltage of approximately 15 kV, and solution flow rate below 2 µL/min.

The diameters of ZnO fibres ranged from 142.7-442.3 nm. In contrast, the fibre diameter found in this study is slightly larger than those which resulted from previous studies, with values ranging from 65.3 to 82.8 nm at the same precursor flow rate [39]. The cause is that the collector used in the previous studies is an aluminium plate with a greater electrical conductivity than that of the FTO glass. The greater the electrical conductivity, the higher the speed the solution precursor was drawn for producing smaller diameter ZnO fibres.

Table 1. Diameter of ZnO fibres.

Size	**Flow rate of precursors**			
	2 µL/min	**4 µL/min**	**6 µL/min**	**8 µL/min**
Mean diameter	142.7	180.3	432.0	442.3
Deviation standard	43.2	57.1	90.5	163.9

Meanwhile, X-ray diffraction spectra of ZnO fibres are shown in Fig. 3. The three main diffraction peaks have indices of (100), (002), and (101) corresponding to the hexagonal structure of ZnO crystals based on JC-PDF 36-1451. The increase in the flow rate of the precursor solution in the synthesis of ZnO fibres with an electrospinning machine does not change the X-ray diffraction pattern, revealing that no new phase was formed. As the precursor flow rates increased, the intensity of the diffraction peaks increased and narrowed the full width at half maximum (FWHM).

Furthermore, the crystalline diameter of ZnO was calculated using the Debye-Scherrer's formula at the highest peak [49]:

$$D = \frac{k\lambda}{\beta \cos\theta} \tag{4}$$

Meanwhile, Williamson and Hall explained that the strain (ε) in the crystal has an effect on the changes in the crystalline size. According to Williamson-Hall equations, crystalline size and strain relationships can be expressed by [50, 51]:

$$\beta \cos\theta = \frac{k\lambda}{D} + 4\epsilon \sin\theta \tag{5}$$

The crystalline sizes of ZnO fibres were calculated with Eqs. (1) and (2) and are shown in Table 2. Meanwhile, the crystallinity of ZnO fibres ranged between 71.07 and 74.28%. In the synthesis of ZnO fibres with the electrospinning machine, the crystalline size was also influenced by the flow rate of precursor solution. The greatest crystalline size of the ZnO fibres occurred at a flow rate of 4 µL/min. The crystalline size of the ZnO fibres also increased because of internal strain. The greatest strain on the ZnO fibres was 0.315% when the flow rate of precursor solution was 4 µL/min.

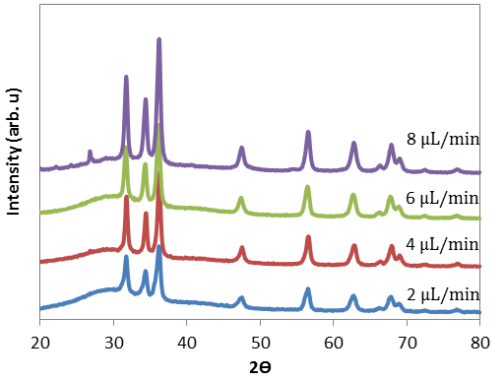

Fig. 3. X-ray diffraction spectra of ZnO fibres.

Table 2. Band gap energy, crystalline size, and crystallinity of ZnO fibres.

Flow rate (µL/min)	Band gap energy (eV)	Crystallinity (%)	Crystalline size (nm)		Strain (%)
			Debye-Scherrer	Williamson-Hall	
2	3.17	73.67	13.9	22.2	0.207
4	3.19	74.28	17.6	45.1	0.315
6	3.22	73.24	15.6	34.6	0.297
8	3.29	71.07	15.5	27.9	0.222

The UV-vis absorption spectra are shown in Fig. 4. The band gap energy of ZnO fibres was calculated by the method of the Tauc plot [52, 53]. The optical band gap energy (E_g) of ZnO fibres was determined from the intercepts with the photon energy (x-axis) by linear fitting of the $(\alpha \cdot h\nu)^2$ vs. $h\nu$ curve, as shown in Fig. 4 [54, 55]. The band gap energy of ZnO fibres calculated by the method of the Tauc plot ranges from 3.17 to 3.29 eV. Similar results can also be observed in some previous studies [55]. Therefore, the flow rate of precursor solution led to an increase in the band gap energy of synthesized ZnO fibres.

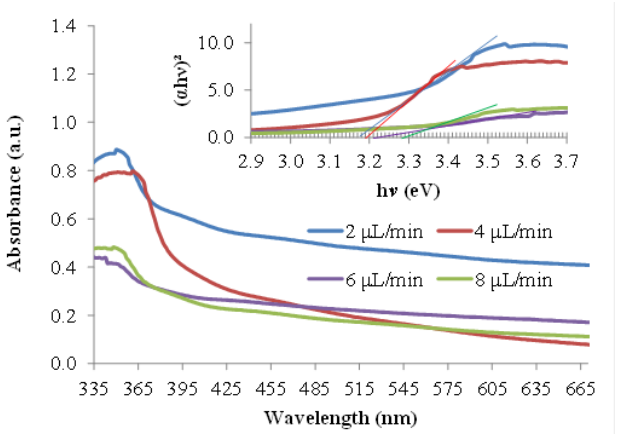

Fig. 4. UV-Vis absorption spectra of ZnO fibres; insert is the curve of $(\alpha h\nu)^2$ versus photon energy ($h\nu$).

3.2. Performance of hybrid NGs (NGs)

A schematic of the hybrid NGs in this research can be seen in Fig. 1. The hybrid NGs were the solar cell of DSSCs, where part of the counter electrode is freely moving with the elasticity obtained from rubber attached onto the back electrode. When exposed to light, the hybrid NGs work as solar cells, and when subjected to the mechanical load, the cells serve as piezoelectric-based NGs.

The characteristics of the current and voltage of the hybrid NGs when exposed to a solar simulator irradiance of 1000 W/m² are shown in Fig. 5. Meanwhile, the performance of the hybrid NGs when subjected to a load of 0.5 kg is shown in Fig. 6.

When the hybrid NGs work as photovoltaics, the open circuit voltage (V_{oc}) generated ranges from 0.421 to 0.507 V. As the flow rate of the solution precursors during the process of electrospinning increases, the generated V_{oc} by NGs experiences a slight decline because of the wider band gap energy from the semiconductor made of ZnO fibres. Furthermore, the J_{sc} of photovoltaic-based hybrid NGs decreased quite sharply with an increasing flow rate of precursor solution during the electrospinning process. This is caused by the size of the ZnO particles. The bigger the size of the fibres, the weaker the bond formed between the semiconductor particles and the dye molecules. One of the main factors influencing J_{sc} is the anchoring or bonding between the semiconductor particles and dye molecules [36, 56]. Photovoltaic-based hybrid NGs generated the highest J_{sc} of 0.993 mA/cm².

In addition, besides the size of fibres, the uniformity of ZnO fibres may also determine the level of J_{sc}. Uniform fibres accelerate the flow of electrons. Furthermore, the uniformity of fibres synthesized by the electrospinning machine has become a major issue apart from the size of fibres [57]. The fill factor (FF) and efficiency of photovoltaic-based hybrid NGs are affected by the flow rate of the precursor solution. The highest efficiency of photovoltaic-based hybrid NGs of 0.24% was produced by a flow rate of 2 µL/min and influenced by the grain size of SnO_2:F in the FTO glass of 470 nm [35]. Better contact may occur between the grains of SnO_2:F (470 nm) and the fibres of ZnO (142.7 nm) produced by a flow rate of 2 µL/min. The appropriate relationship between the grain size of SnO_2:F and the fibre size of ZnO provides good and strong bonding, thus enhancing the transfer of electrons.

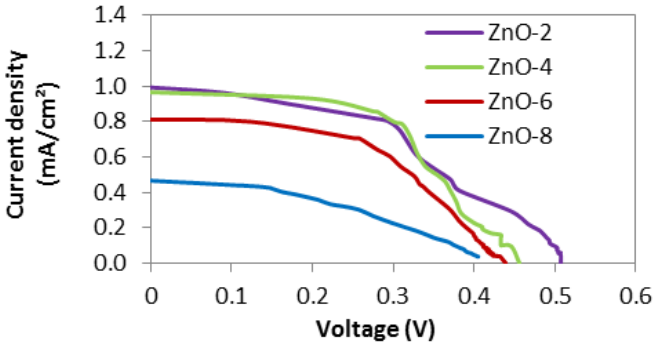

Fig. 5. I-V curves of photovoltaic-based hybrid NGs.

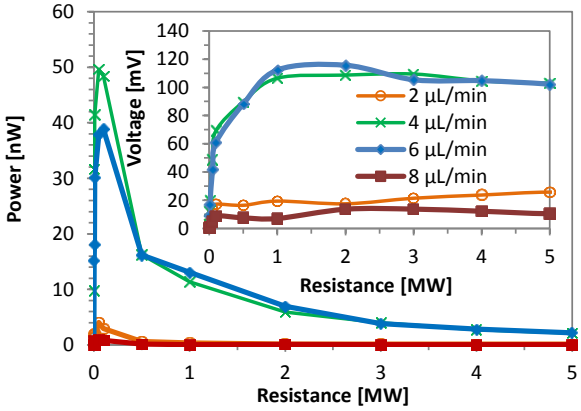

Fig. 6. Output power of piezoelectric-based hybrid NGs.

Meanwhile, the highest output power from the ZnO fibre-based hybrid NGs was also higher than that of the lead zirconate titanate (PZT) fibre-based NGs. The highest output power of the lead zirconate titanate (PZT) fibre-based NGs was 30 nW at 6 MΩ [38].

Next, the NGs were tested for their ability to produce electricity from the mechanical load as shown in Fig. 5. The highest output voltage and power were 352 mV and 48.2 nW, respectively, when the ZnO fibres were synthesized by an electrospinning machine at a flow rate of 4 µL/min. The output voltage of ZnO fibre-based hybrid NGs was higher than that of ZnO-PSS/PVA thin layer-based NGs (varying from 10 to 100 mV) [58].

Moreover, the output voltage and power are strongly affected by the positions of Zn and O atoms in a hexagonal structure of ZnO because the dipole moment is generated from the difference in the electronegativity and positions of these two atoms. The ZnO fibres in the hybrid NGs exhibited internal strains in their crystal structure influencing the increase of their size compared to the size of the crystal without strain, as seen in Table 2. The existence of a greater strain stretched apart the positions of both of the atoms, and therefore, the output voltage increased.

Generally, the highest power generated from photovoltaic-based hybrid NGs is still far greater than that generated from piezoelectric-based hybrid NGs. The highest powers generated from photovoltaic- and piezoelectric-based hybrid NGS are 706.72 µW and 49.6 nW, respectively, as shown in Fig. 6. Therefore, the power densities of 706.72 µW/cm² and 49.6 nW/cm² are very promising for self-powered devices based on hybrid NGs. However, the power density of piezoelectric-based hybrid NGs needs to be enhanced by means of doping the ZnO fibres with suitable materials.

4. Conclusions

Hybrid NGs were successfully fabricated and investigated. Hybrid-NGs work by using photovoltaic and piezoelectric principles. Piezoelectric-based NGs work when subjected to mechanical loads, while photovoltaic-based NGs work upon

receiving light irradiation. The semiconductor used was ZnO fibres synthesized by an electrospinning machine with various flow rates of precursor solution from 2 to 8 μL/min. The crystallinity, crystalline size, fibre size, and fibre uniformity were strongly affected by the flow rate of the precursor solution. Meanwhile, the voltage and power generated from hybrid NGs were influenced by the crystalline quality and morphology of the ZnO fibres. The voltage and power generated from photovoltaic-based hybrid NGs are still far higher when compared to those generated from the piezoelectric-based hybrid NGs. The highest voltages of photovoltaic- and piezoelectric-based NGs were 507 and 36.3 mV, respectively. Meanwhile, the maximum powers of photovoltaic- and piezoelectric-based NGs were 706.72 μW and 49.6 nW, corresponding to power densities of 706.72 μW/cm² and 49.6 nW/cm², respectively. To enhance the performance of hybrid NGs, the properties of the ZnO fibres need to be improved by doping with suitable dopant materials. By doing so, the hybrid-NGs become suitable for fabrication into devices of self-powered NGs.

Acknowledgements

The authors thank the Rector of Universitas Sebelas Maret, Nr: 353 /UN27.21/PN/2016 and General Director of Strengthening Research and Development, Ministry of Research, Technology, and Higher Education, the Republic of Indonesia, Nr: 041/SP2H/LT/DRPM/II/2016, 17 February 2016 and Nr: 01/E/KPT/2017, 6 January 2017 for supporting the funding for doing the research.

References

1. Wang, Z.L. (2008). Towards self-powered nanosystems: From nanogenerators to nanopiezotronics. *Advanced Functional Materials*, 18(22), 3553-3567.
2. Wang, Z.L.; Wang, X.; Song, J.; Liu, J.; and Gao, Y. (2008). Piezoelectric nanogenerators for self-powered nanodevices. *IEEE Computer Society*, 7(1), 49-55.
3. Chang, C.; Tran, V.H.; Wang, J.; Fuh, Y.K.; and Lin, L. (2010). Direct-write piezoelectric polymeric nanogenerator with high energy conversion efficiency. *Nano Letters*, 10(2), 726-731.
4. Park, K.I.; Xu, S.; Liu, Y.; Hwang, G.T.; L, K.S.J.; Wang, Z.L.; and Lee, K.J. (2010). Piezoelectric $BaTiO_3$ thin film nanogenerator on plastic substrates. *Nano letters*, 10(12), 4939-4943.
5. Chung, S.Y.; Kim, S.; Lee, J.-H.; Kim, K.; Kim, S.-W.; Kang, C.-Y.; Yoon, S.-J.; and Kim, Y.S. (2012). All solution processed flexible thin film piezoelectric nanogenerator. *Advanced Materials*, 24(45), 6022-6027.
6. Yang, Y.; Wang, S.; Zhang, Y.; and Wang, Z.L. (2012). Pyroelectric nanogenerators for driving wireless sensors. *Nano letters*, 12(12), 6408-6413.
7. Kwon, J.; Sharma, B.K.; and Ahn, J.-H. (2013). Graphene based nanogenerator for energy harvesting. *Japanese Journal of Applied Physics*, 52(6S), 06GA02:01-09.

8. No, I.-J.; Jeong, D.-Y.; Lee, S.; Kim, S.-H.; Cho, J.-W.; and Shin, P.-K. (2013). Enhanced charge generation of the ZnO nanowires/PZT hetero-junction based nanogenerator. *Microelectronic Engineering*, 110, 282-287.
9. Stassi, S.; Cauda, V.; Ottone, C.; Chiodoni, A.; Pirri, C.F.; and Canavese, G. (2015). Flexible piezoelectric energy nanogenerator based on ZnO nanotubes hosted in a polycarbonate membrane. *Nano Energy*, 13(April 2015), 474-481.
10. Yin, B.; Qiu, Y.; Zhang, H.; Lei, J.; Chang, Y.; Ji, J.; Luo, Y.; Zhao, Y.; and Hu, L. (2015). Piezoelectric performance enhancement of ZnO flexible nanogenerator by a nio-zno p-n junction formation. *Nano Energy*, 14, 95-101.
11. Pan, C.; Li, Z.; Guo, W.; Zhu, J.; and Wang, Z.L. (2011). Fibre-based hybrid nanogenerators for/as self-powered systems in biological liquid. *Angewandte Chemie (International ed. in English)*, 50(47), 11192-11196.
12. Kathalingam, A.; Valanarasu, S.; Senthilkumar, V.; and Rhee, J.-K. (2013). Piezo and photoelectric coupled nanogenerator using CdSe quantum dots incorporated ZnO nanowires in ITO/ZnO NW/Si structure. *Materials Chemistry and Physics*, 138(1), 262-269.
13. Zhong, H.; Wu, Z.; Li, X.; Xu, W.; Xu, S.; Zhang, S.; Xu, Z.; Chen, H.; and Lin, S. (2016). Graphene based two dimensional hybrid nanogenerator for concurrently harvesting energy from sunlight and water flow. *Carbon*, 105, 199-204.
14. Sinha, N.; Ray, G.; Godara, S.; Gupta, M.K.; and Kumar, B. (2014). Enhanced piezoelectric output voltage and ohmic behavior in Cr-doped ZnO nanorods. *Materials Research Bulletin*, 59(November 2014), 267-271.
15. Li, W.; Li, P.; Zeng, H.; Hao, J.; and Zhai, J. (2015). Enhanced dielectric and piezoelectric properties in lead-free $Bi_{0.5}Na_{0.5}$ TiO_3-$BaTiO_3$-$SrTiO_3$ thin films with seed layer. *Ceramics International*, 41(1), S356-S360.
16. Karan, S.K.; Mandal, D.; and Khatua, B.B. (2015). Self-powered flexible Fe-doped RGO/PVDF nanocomposite: An excellent material for a piezoelectric energy harvester. *Nanoscale*, 7(24), 10655-10666.
17. Sumang, R.; Wicheanrat, C.; Bongkarn, T.; and Maensiri, S. (2015). High densification and dielectric properties of lead-free $(K_{0.5}Na_{0.5})NbO_3$ piezoelectric ceramics with optimum excess Na_2O and K_2O contents. *Ceramics International*, 41(Supplement 1, July 2015), S136-S142.
18. Grätzel, M. (2001). Photoelectrochemical cells. *Nature*, 414(6861), 338-344.
19. Yang, Z.; Xu, T.; Ito, Y.; Welp, U.; and Kwok, W.K. (2009). Enhanced electron transport in dye-sensitized solar cells using short ZnO nanotips on a rough metal anode. *The Journal of Physical Chemistry C*, 113(47), 20521-20526.
20. Kim, K.S.; Kang, Y.S.; Lee, J.H.; Shin, Y.J.; Park, N.G.; Ryu, K.S.; and Chang, S.H. (2006). Photovoltaic properties of nano-particulate and nanorod array ZnO electrodes for dye-sensitized solar cell. *Bulletin Korean Chemical Society*, 27(2), 295-298.
21. Suri, P.; Panwar, M.; and Mehra, R.M. (2007). Photovoltaic performance of dye-sensitized ZnO solar cell based on Eosin-y photosensitizer. *Materials Science-Poland*, 25(1), 137-144.
22. Kashyout, A.B.; Soliman, H.M.; Hassan, H.S.; and Abousehly, A.M. (2010). Frabrication of ZnO and ZnO:Sb nanoparticles for gas sensor applications. *Journal of Nanomaterials*, 2010, 1-8.

23. Wang, L.; Kang, Y.; Liu, X.; Zhang, S.; Huang, W.; and Wang, S. (2012). ZnO nanorod gas sensor for ethanol detection. *Sensors and Actuators B: Chemical*, 162(12), 237-243.
24. Lee, S.H.; Lee, S.S.; Choi, J.-J.; Jeon, J.U.; and Ro, K. (2005). Fabrication of a ZnO piezoelectric micro cantilever with a high-aspect-ratio nano tip. *Microsystem Technologies*, 11(6), 416-423.
25. Lin, R.-C.; Chen, Y.-C.; and Kao, K.-S. (2007). Two-step sputtered ZnO piezoelectric films for film bulk acoustic resonators. *Applied Physics A: Materials Science & Processing*, 89(2), 475-479.
26. Pan, M.-C.; Wu, T.-H.; Bui, T.-A.; and Shih, W.-C. (2012). Fabrication of highly c-axis textured ZnO thin films piezoelectric transducers by RF sputtering. *Journal of Materials Science: Materials in Electronics*, 23(2), 418-424.
27. Wang, Z.L. (2007). Novel nanostructures of ZnO for nanoscale photonics, optoelectronics, piezoelectricity, and sensing. *Applied Physics A: Materials Science & Processing*, 88(1), 7-15.
28. Yoon, M.-S.; Kim, Y.-M.; Kweon, S.-Y.; ·, T.-W.H.; Lee, Y.-G.; Ryu, S.-L.; Kim, I.-H.; Kim, H.-J.; and Ur, S.-C. (2006). Effects of ZnO on the piezoelectric properties of $Pb(Mn_{1/3}\ Sb_{2/3})O_3$-$Pb(Zr,Ti)O_3$ ceramics. *Journal of Electroceramics*, 17(2-4), 635-637.
29. Lee, D.Y.; Kim, H.; Li, H.M.; Jang, A.R.; Lim, Y.D.; Cha, S.N.; Park, Y.J.; Kang, D.J.; and Yoo, W.J. (2013). Hybrid energy harvester based on nanopillar solar cells and PVDF nanogenerator. *Nanotechnology*, 24(17), 175402.
30. Lee, K.Y.; Gupta, M.K.; and Kim, S.-W. (2015). Transparent flexible stretchable piezoelectric and triboelectric nanogenerators for powering portable electronics. *Nano Energy*, 14(May 2015), 139-160.
31. Yoon, G.C.; Shin, K.-S.; Gupta, M.K.; Lee, K.Y.; Lee, J.-H.; Wang, Z.L.; and Kim, S.-W. (2015). High-performance hybrid cell based on an organic photovoltaic device and a direct current piezoelectric nanogenerator. *Nano Energy*, 12, 547-555.
32. 32. Kim, D.Y.; Lee, S.; Lin, Z.-H.; Choi, K.H.; Doo, S.G.; Chang, H.; Leem, J.-Y.; Wang, Z.L.; and Kim, S.-O. (2014). High temperature processed ZnO nanorods using flexible and transparent mica substrates for dye-sensitized solar cells and piezoelectric nanogenerators. *Nano Energy*, 9(October 2014), 101-111.
33. Park, J.-A.; Moon, J.; Lee, S.-J.; Lim, S.-C.; and Zyung, T. (2009). Fabrication and characterization of ZnO nanofibres by electrospinning. *Current Applied Physics*, 9(3), S210-S212.
34. Ren, H.; Ding, Y.; Jiang, Y.; Xu, F.; Long, Z.; and Zhang, P. (2009). Synthesis and properties of ZnO nanofibres prepared by electrospinning. *Journal of SolGel Science and Technology*, 52(2), 287-290.
35. Suyitno; Zainal, A.; Ahmad, A.S.; Argatya, T.S.; and Ubaidillah (2014). Optimization parameters and synthesis of fluorine doped tin oxide for dye-sensitized solar cells. *Applied Mechanics and Materials*, 575, 689-695.
36. Suyitno, S.; Saputra, T.J.; Supriyanto, A.; and Arifin, Z. (2015). Stability and efficiency of dye-sensitized solar cells based on papaya-leaf dye.

Spectrochimica Acta - Part A: Molecular and Biomolecular Spectroscopy, 148(5 September 2015), 99-104.

37. Choi, D.; Lee, K.Y.; Lee, K.H.; Kim, E.S.; Kim, T.S.; Lee, S.Y.; Kim, S.-W.; Choi, J.-Y.; and Kim, J.M. (2010). Piezoelectric touch-sensitive flexible hybrid energy harvesting nanoarchitectures. *Nanotechnology*, 21(40), 405503.
38. Chen, X.; Xu, S.; Yao, N.; and Shi, Y. (2010). 1.6 V nanogenerator for mechanical energy harvesting using PZT nanofibres. *Nano Letters*, 10(6), 2133-2137.
39. Suyitno; Purwanto, A.; Hidayat, R.L.L.G.; Sholahudin, I.; Yusuf, M.; Huda, S.; and Arifin, Z. (2014). Fabrication and characterization of zinc oxide-based electrospun nanofibres for mechanical energy harvesting. *Journal of Nanotechnology in Engineering and Medicine*, 5(1), 011002.
40. Yang, X.; Shao, C.; Guan, H.; Li, X.; and Gong, J. (2004). Preparation and characterization of ZnO nanofibres by using electrospun PVA/zinc acetate composite fibre as precursor. *Inorganic Chemistry Communications*, 7, 176-178.
41. Sangkhaprom, N.; Supaphol, P.; and Pavarajarn, V. (2010). Fibrous zinc oxide prepared by combined electrospinning and solvothermal techniques. *Ceramics International*, 36(1), 357-363.
42. Lee, J.S.; Choi, K.H.; Ghim, H.D.; Kim, S.S.; Chun, D.H.; Kim, H.Y.; and Lyoo, W.S. (2004). Role of molecular weight of atactic poly(vinyl alcohol) (PVA) in the structure and properties of pva nanofabric prepared by electrospinning. *Journal of Applied Polymer Science*, 93(4), 1638-1646.
43. Chatterjee, S.K.; Sethi, K.R.; and Riess, G. (1987). Interpolymer complexes: Study of interaction of polyvinylpyrrolidone) with p-hydrqxybenzoic acid-formaldehyde copolymer in nonaqueous media. *Journal of Macromolecular Science: Part A - Chemistry*, 24(8), 859-868.
44. Wu, X.; Zhao, Y.; Yang, C.; and He, G. (2015). PVP-assisted synthesis of shape-controlled $CuFeS_2$ nanocrystals for Li-ion batteries. *Journal of Materials Science*, 50(12), 4250-4257.
45. Koczkur, K.M.; Mourdikoudis, S.; Polavarapu, L.; and Skrabalak, S.E. (2015). Polyvinylpyrrolidone (PVP) in nanoparticle synthesis. *Dalton Transactions*, 44(41), 17883-17905.
46. Rojas, O.J.; Montero, G.A.; and Habibi, Y. (2009). Electrospun nanocomposites from polystyrene loaded with cellulose nanowhiskers. *Journal of Applied Polymer Science*, 113(2), 927-935.
47. Thompson, C.J.; Chase, G.G.; Yarin, A.L.; and Reneker, D.H. (2007). Effects of parameters on nanofibre diameter determined from electrospinning model. *Polymer*, 48(23), 6913-6922.
48. Doh, S.J.; Kim, C.; Lee, S.G.; Lee, S.J.; and Kim, H. (2008). Development of photocatalytic TiO_2 nanofibres by electrospinning and its application to degradation of dye pollutants. *Journal of Hazardous Materials*, 154(1-3), 118-127.
49. Pongwan, P.; Inceesungvorn, B.; and Wetchakun, K. (2012). Highly efficient visible-light-induced photocatalytic activity of Fe-doped TiO_2 nanoparticles. *Engineering Journal*, 16(3), 143-151.

50. Mote, V.; Purushotham, Y.; and Dole, B. (2012). Williamson-hall analysis in estimation of lattice strain in nanometer-sized ZnO particles. *Journal of Theoretical and Applied Physics*, 6(6), 1-8.
51. Kour, P.; and Sinha, S.K. (2013). Studies of Sr^{2+} ion substitution on ferroelectric and piezoelectric properties of PZT nanocrystalline. *Cerâmica*, 59(349), 34-38.
52. Viezbicke, B.D.; Patel, S.; Davis, B.E.; and Birnie, D.P. (2015). Evaluation of the tauc method for optical absorption edge determination: ZnO thin films as a model system. *Physical Status Solidi B*, 252(8), 1700-1710.
53. Rahman, M.M.; Khan, M.K.R.; Islam, M.R.; Halim, M.A.; Shahjahan, M.; Hakim, M.A.; Saha, D.K.; and Khan, J.U. (2012). Effect of Al doping on structural, electrical, optical and photoluminescence properties of nano-structural ZnO thin films. *Journal of Materials Science & Technology*, 28(4), 329-335.
54. Hung-Chun Lai, H.; Basheer, T.; Kuznetsov, V.L.; Egdell, R.G.; Jacobs, R.M.J.; Pepper, M.; and Edwards, P.P. (2012). Dopant-induced bandgap shift in Al-doped ZnO thin films prepared by spray pyrolysis. *Journal of Applied Physics*, 112(8), 083708.
55. Huang, B.; Zhao, C.; Zhang, M.; Zhang, Z.; Xie, E.; Zhou, J.; and Han, W. (2015). Doping effect of In_2O_3 on structural and ethanol-sensing characteristics of ZnO nanotubes fabricated by electrospinning. *Applied Surface Science*, 349, 615-621.
56. Ooyama, Y.; and Harima, Y. (2012). Photophysical and electrochemical properties, and molecular structures of organic dyes for dye-sensitized solar cells. *ChemPhysChem*, 13(18), 4032-4080.
57. Suyitno; Huda, S.; Arifin, Z.; and Hadi, S. (2014). Repeatability, reproducibility, and durability of zinz oxide fibre-based nanogenerator synthesized by simple electrospinning machine. *Advanced Science Letters*, 20(10-12), 2299-2303.
58. Loh, K.J.; and Chang, D. (2011). Zinc oxide nanoparticle-polymeric thin films for dynamic strain sensing. *Journal of Materials Science*, 46(1), 228-237.